Journal Pre-proof

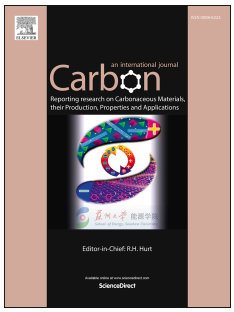

Defect-induced photocurrent gain for carbon nanofilm-based broadband infrared photodetector

Xiaoxue Cao, Li Peng, Lixiang Liu, Jianhang Lv, Zongwen Li, Feng Tian, Yunfan Dong, Xinyu Liu, Ying Shen, Haiyan Sun, Yang Xu, Wenzhang Fang, Chao Gao

PII: S0008-6223(22)00553-X

DOI: https://doi.org/10.1016/j.carbon.2022.07.028

Reference: CARBON 17360

To appear in: *Carbon*

Received Date: 16 May 2022

Revised Date: 1 July 2022

Accepted Date: 11 July 2022

Please cite this article as: X. Cao, L. Peng, L. Liu, J. Lv, Z. Li, F. Tian, Y. Dong, X. Liu, Y. Shen, H. Sun, Y. Xu, W. Fang, C. Gao, Defect-induced photocurrent gain for carbon nanofilm-based broadband infrared photodetector, *Carbon* (2022), doi: https://doi.org/10.1016/j.carbon.2022.07.028.

This is a PDF file of an article that has undergone enhancements after acceptance, such as the addition of a cover page and metadata, and formatting for readability, but it is not yet the definitive version of record. This version will undergo additional copyediting, typesetting and review before it is published in its final form, but we are providing this version to give early visibility of the article. Please note that, during the production process, errors may be discovered which could affect the content, and all legal disclaimers that apply to the journal pertain.

© 2022 Published by Elsevier Ltd.

Xiaoxue Cao: Design and conduct the experiments, Interpreted the data, Writing - Review & Editing the manuscript.

Li Peng: Degradation experiment, Analyzed the data, Revised the manuscript.

Lixiang Liu: Degradation experiment, Analyzed the data, Revised the manuscript.

Jianhang Lv: Degradation experiment, Analyzed the data, Revised the manuscript.

Zongwen Li: Revised the manuscript.

Feng Tian: Revised the manuscript.

Yunfan Dong: Revised the manuscript.

Xinyu Liu: Revised the manuscript.

Ying Shen: Revised the manuscript.

Haiyan Sun: Revised the manuscript.

Wenzhang Fang: Propose the study concept, Revised the manuscript

Yang Xu: Supervision, Project administration, Funding acquisition.

Chao Gao: Supervision, Project administration, Funding acquisition.

Journal Pre-proof

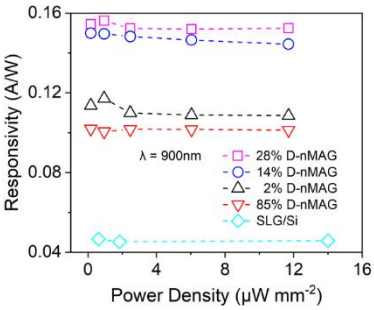

The responsivity of D-nMAG/Si at 900 nm

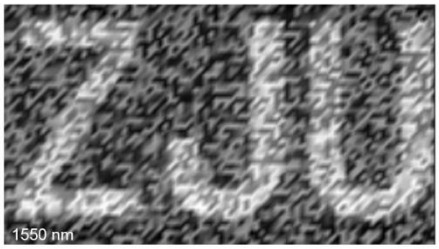

1550 nm wavelength; 2 mW/mm^2 power density

The photograph of "ZJU" imaged by line array device

Journal Pre-proof

Defect-induced Photocurrent Gain for Carbon Nanofilm-based Broadband Infrared Photodetector

Xiaoxue Cao [a, b], Li Peng [b], Lixiang Liu [a], Jianhang Lv [a], Zongwen Li [a], Feng Tian [a], Yunfan Dong [a], Xinyu Liu [a], Ying Shen [b], Haiyan Sun [c], Yang Xu [a*], Wenzhang Fang [b*], Chao Gao [b*]

[a] *School of Micro-nanoelectronics, State Key Laboratory of Silicon Materials, Hangzhou Global Scientific and Technological Innovation Center (HIC), ZJU-UIUC Joint Institute, Zhejiang University, Hangzhou, 310000, China*

[b] *MOE Key Laboratory of Macromolecular Synthesis and Functionalization, Department of Polymer Science and Engineering, International Research Center for X Polymers, Zhejiang University, Hangzhou, 310000, China*

[c] *Hangzhou Gaoxi Technol Co Ltd, Hangzhou 310027, China.*

Keywords: IR photodetector; graphene nanofilm; wafer-scale; defective structure; photocurrent gain

ABSTRACT

Broad-spectrum detection and large-scale integration are the inevitable trends in the current evolution of infrared photodetectors. New materials were integrated with existing platforms to further improve the performance of infrared photodetectors. Here, we reported a defective macro-assembled graphene nanofilm (D-nMAG)/Silicon (Si) photodetector using trap-assisted gain to

* Corresponding author. Tel: 0571 8795-2088. E-mail: chaogao@zju.edu.cn (Chao Gao); E-mail: wenzhang.fang@zju.edu.cn (Wenzhang Fang); E-mail: yangxu-isee@zju.edu.cn (Yang Xu).

Journal Pre-proof

optimize the photoelectric response. This wafer-scale environmentally friendly carbon material can be easily compatible with the complementary-metal-oxide-semiconductor (CMOS) technical. Noteworthy, the defective states in D-nMAG trap carriers and then enter the conduction (CB) and valence band (VB) again to be thermalized, generating a gain in photocurrent. Thus, our D-nMAG-based line array image sensor exhibits high-resolution infrared imaging of the target. This device displays a high responsivity at room temperature within a broad-spectrum region, *i.e.*, 0.156 A/W @ 900 nm in the near-infrared (NIR) region and 3.7 mA/W @ 4 μm in the mid-infrared (MIR) region. Our work provides a carbon nanofilm for IR detection at a broad-spectrum region, with tunable defective structure, uniform thickness, and wafer-scale production.

1. Introduction

With the continuous advancement of materials and device structures, infrared photodetectors have been effectively used in industry, science, the military, and daily life[1-3]. Nevertheless, as the demand for practical applications evolves, researchers are engaged in finding new materials and integrating them with existing platforms to push the limits of the energy efficiency of conventional infrared photodetectors[4-10]. For instance, III-V semiconductor (*e.g.*, InAs, GaAs) quantum dots and quantum-well-based structures revolutionalized high-performance infrared photoelectric detection[11]. Nevertheless, the spectral range for photodetection is limited by the bandgap of the quantum dots or the quantum well. The response time is tens of milliseconds or even up to a few seconds because of the slow charge diffusion process. Although III-V semiconductor-based photodetectors have extended the detection bandwidth to the mid-infrared range, these junctions still suffer from low detection rates (D*), especially at room temperature[12]. In addition, ill-defined barrier heights and Fermi level pinning due to metal-induced gap states further worsen the signal-to-noise ratio (SNR)[13, 14].

Recently, considerable works have been reported around carbon-based optoelectronics due to the unique physical structure, chemical stability, and green synthesis of carbon materials[15]. Graphene is considered one of the most promising candidates for optoelectronic materials for its superior optical and electrical properties[16-19]. Single-layer graphene (SLG) shows only 2.3% light absorption, limiting its application in infrared detection[20]. Our previous work proposed a macro-assembled graphene nanofilm (nMAG) with uniform and controllable thickness and high crystalline orientation through a wafer-scale preparation process. The nMAGs raise the light absorption to 45% in the wavelength ranging from 2 to10 μm and drastically broaden the detection range of graphene-based infrared detectors[21-23]. However, the fabrication of highly crystallized AB-stacked nMAG required high-temperature thermal treatment (2 h of sintering at 2800 ^{o}C in the argon atmosphere), which significantly increases energy consumption and production cost.

Nevertheless, nMAG/Si suffers from low photodetection. Recently, some works have reported that trapped carriers can be thermally re-excited to the conduction band (CB) or valence band (VB) of the materials, thus leading to the re-establishment of carrier equilibrium and the gain of the photocurrent[24-26]. It is difficult to tune the defect states for conventional bulk materials because the modulation of semiconductor trap states is mainly concentrated on surface/interface treatments[27, 28]. 2D materials afford an excellent platform to explore these issues[29, 30] because their electronic properties can be flexibly modulated by defect and interface engineering to attain a high photoelectric transformation rate[31-35]. Numerous techniques have triggered defect engineering in 2D materials, including electron beams (e-beams), plasma, chemical treatment, ozone, and laser. To further improve the infrared detection performance of the carbon-based device, we modulate the material structure to evaluate the effect of material defect states on device performance.

We propose a macro-assembled graphene nanofilm with tunable defect states (D-nMAG) for broadband infrared photodetection and explore the relationship between defect sates content and the photodetection. We synthesized D-nMAG through thermal treatment at a low temperature and enhanced the responsivity of the device by introducing defects to the carbon materials simultaneously. Based on the outstanding characteristics of controllable uniform thickness and strong light absorption in ultra-wide spectral range, high-performance D-nMAG/Si photodetectors were established in this work. Defect states were fully utilized to achieve an ultra-fast (~132 ns) broad spectral response with high responsivity in NIR (0.156 A/W @ 900 nm) and MIR (3.7 mA/W @ 4 μm). The carbon-based defective materials can be fabricated at a large scale and are easily compatible with the CMOS technical. These findings provide a solid approach for nanofilm modifications and a theoretical basis for constructing low-cost, high-performance, broad-spectrum infrared photodetectors.

2. Experimental

2.1 Material Characterization

The Raman spectrum was measured by Renishaw inVia-Reflex Raman microscope with a 532-nm laser. The scanning electron microscopy (SEM) images were taken on a field-emission SEM system (Hitachi S4800) at an acceleration voltage of 5 kV. The transmission electron microscopy (TEM) images were obtained on a Hitachi H-9500 instrument operating at 300 kV. We tested the X-ray photoelectron spectroscopy (XPS) by PHI 5000C ESCA System operated at 14.0 kV.

2.2 Device Fabrication

We fabricated D-nMAG/Si devices using 500-μm-thick, lightly-n-doped (10^{15} cm^{-3}) silicon substrates with a 300 nm SiO_2 dielectric layer. The schematic of the device fabrication is shown

in **Fig. S1**. We spin-coated photoresist (model AR-P 5350) on the substrate, then used the Aligner 12016042 UV lithography to pattern electrode graphics and sputtered Cr/Au (5/60 nm) on the top layer using Sputter 19002923 Magnetron Sputtering System (DISCOVERY-635). After lift-off, we spin-coated photoresist (model AR-P 5350) on the substrate surface. Then the silicon window was patterned with a size of 1×1 mm^2 using UV lithography. Then the oxide layer was removed from the silicon window by wet etching silicon dioxide in buffered oxide etch (BOE). After etching the oxide layer of the silicon window, the device is placed in acetone and isopropanol to remove the photoresist. Then D-nMAG was directly transferred to a silicon window by tweezers and affixed with water assistance, forming a clean boundary heterojunction with van der Waals contacts. Photolithography further patterned the device to etch the D-nMAG outside the electrode by Inductively Coupled Plasma Dry Etching System (OXFORD, Plasmapro100 Cobra 180). Finally, ohmic contact was obtained by GaIn at the back-side of silicon. Au wires were then bonded with the top and back electrodes.

2.3 Device Characterization

The I-V curves were tested by Keithley source meter 2450. The IR light was provided by a laser E2 Fiber-Coupled Optoelectronic Test Probe Station (900 nm), 1064nm, 1342 nm, and a periodic pulse laser (Light Conversion, OPA-Series, 1 to 10 μm, 200 fs pulse width, and 100 kHz repetition rate). Infrared bandpass filters (FB2000-500 to FB4000-500, Thorlabs) were used to filter the stray light from the MIR laser. The femtosecond transient absorption setup used for this study was based on a PHAROS laser system (Light Conversion, 1030 nm, < 190 fs, 200 μJ/pulse, and 100 kHz repetition rate), equipped with nonlinear frequency mixing techniques and the Femto-TA100 spectrometer (Time-Tech Spectra).

Journal Pre-proof

3. Results and discussion

3.1 Preparation method and properties characterization of D-nMAG

We have prepared a wafer-scaled nMAG with uniform and controllable thickness through filtration and calcination processes (**Fig. 1a**). Graphene nanofilms grown by chemical vapor deposition (CVD) face the challenge of uniformity while the thickness is over two layers. Another issue is the existence of a substrate for graphene growth, making it difficult to tune the graphene structure by subsequent processes such as calcination. However, the reduced graphene oxide (rGO) nanofilms in this work can be easily peeled off from the anodic aluminum oxide (AAO) membrane and keep freestanding without any substrate, providing an opportunity for structure reforming and defect tuning. Moreover, the defect content of D-nMAG can be controlled by adjusting the sintering temperature and time[23]. The freestanding rGO films were heated in the Ar atmosphere at 300 ºC (heating rate 1 ºC min^{-1}) for 2 h and then to 1600 ºC or 2000 ºC (heating rate 10 ºC min^{-1}) for different times. The degree of defects in D-nMAG has been attested from the change of D-peak in Raman spectra which is defined by the ratio of the intensity of D peak and G peak (I_D/I_G), as well as the carbon to oxygen ratio in XPS spectra (**Fig. 1b** and **c**). D-nMAG with defect ratios of 85%, 28%, and 14% were fabricated by sintering at 1600 ºC under argon protection for 1 min, 30 min, and 8 h, respectively, while D-nMAG with a defect ratio of 2% was obtained by sintering at 2000 ºC for 2 h.

Moreover, the sheet resistance of D-nMAG also increases with the defect content (**Fig. 1d**). Thus, according to the time-temperature equivalent principle, which means the properties of materials can be controlled as a function of time and temperature[36-38], D-nMAG with controllable thickness (**Fig. S2e** and **Table. 1**) and tunable defect states can be achieved at a relatively low temperature. In our previous work, the fabrication of highly crystallized AB-stacked

nMAG required high-temperature thermal treatment (2 h of sintering at 2800 ºC in the argon atmosphere), which significantly increases energy consumption and production cost. Therefore, we synthesized D-nMAG through thermal treatment at a low temperature and enhanced the responsivity of the device by introducing defects to the carbon materials simultaneously.

Pump-probe transient absorption measurements[22] investigated the hot-carriers dynamic to investigate the intrinsic defect engineering of D-nMAG. **Fig. 1f** illustrates the pump-probe transient absorption with a pump laser of 3.5 μm and a probe laser of 1.2-1.6 μm. The carrier relaxation time of D-nMAG with different defect state contents (~ 2.6 ps) does not differ much (**Fig. 1e**) but is 2 times higher than that of SLG (0.75 ps, **Fig. S3**)[39, 40]. Compared with SLG, a 45 nm-D-nMAG consists of ~120 layers of the graphene sheet[22, 23]. Thus, the interfacial scattering between the hot carriers and substrate in D-nMAG is reduced, generating many hot electrons with higher energy[41, 42]. Moreover, the decoupled electronic structure of D-nMAG enhances the phonon scattering of carriers in the out-of-plane direction, significantly reducing the hot electron cooling time and eventually generating high-energy hot carriers with a long relaxation time[43-46]. The photogenerated carriers are effectively decoupled from crystal lattice for long distances and thus allow more hot carriers to reach the D-nMAG/Si interface[21]. D-nMAG has 45% light absorption (**Fig. S4**) over a wide wavelength range due to increased thickness and hot carriers with higher energy and longer relaxation time than SLG, which is a promising optoelectronic material.

Journal Pre-proof

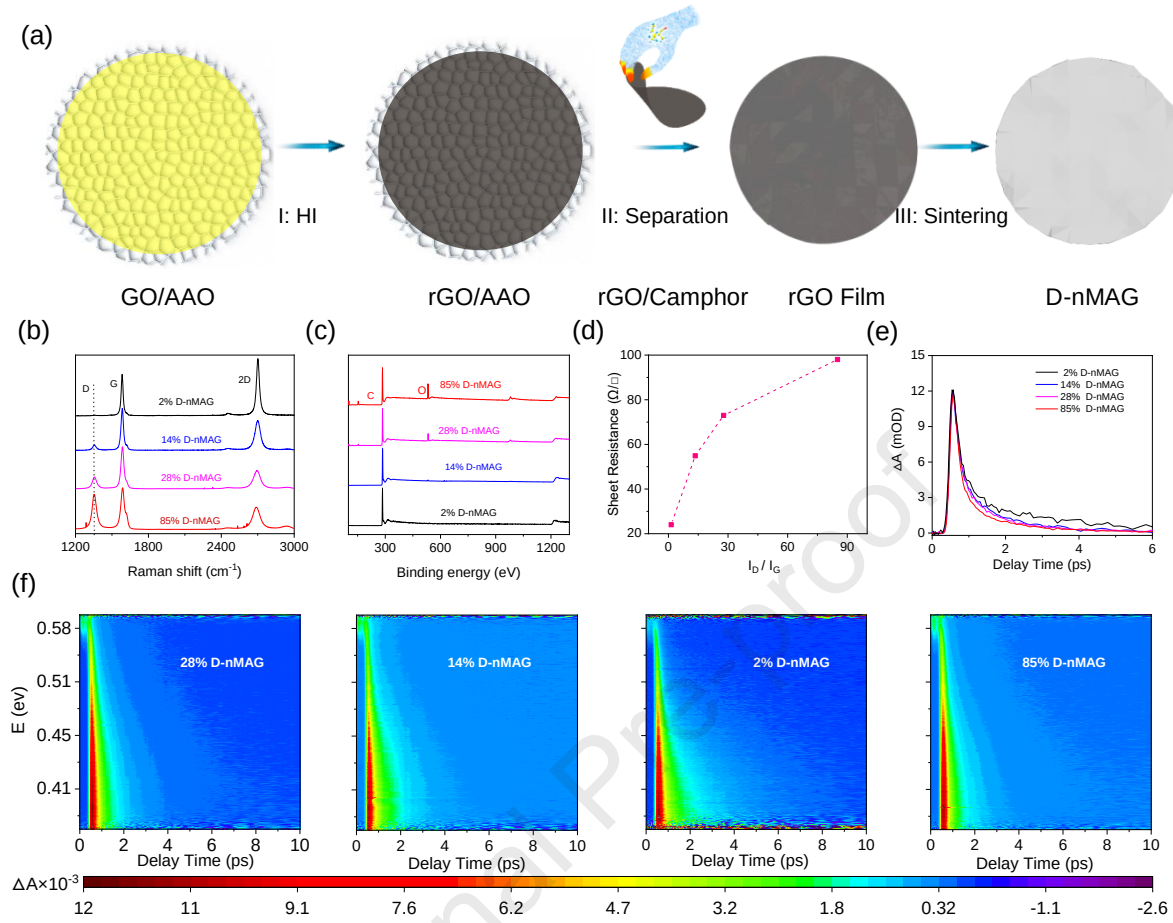

Fig. 1. Preparation method and properties characterization of D-nMAG. (a) Schematic illustration of the D-nMAG preparation process. HI: hydroiodic acid. (b) Raman spectra of nMAG with different content of defect states (85%, 28%, 14% and 2%). The content of defect states was defined by the ratio of the intensity of the D peak and G peak (I_D/I_G). (c) XPS of D-nMAG (85% D-nMAG, O/C = 57.4%; 28% D-nMAG, O/C = 33%; 14% D-nMAG, O/C = 15.4%; 2% D-nMAG, O/C = 0). (d) Sheet resistance as a function of the defect states the content of D-nMAG. (e) The normalized differential transmissivity of D-nMAG/Si as a function of probe delay time. (f) 2D transient absorption mapping of D-nMAG/Si as functions of probe delay time and the half of the incident photon energy with the same vertical coordinates. The sample is pumped at 3.5 μm under 1 mW mm^{-2}.

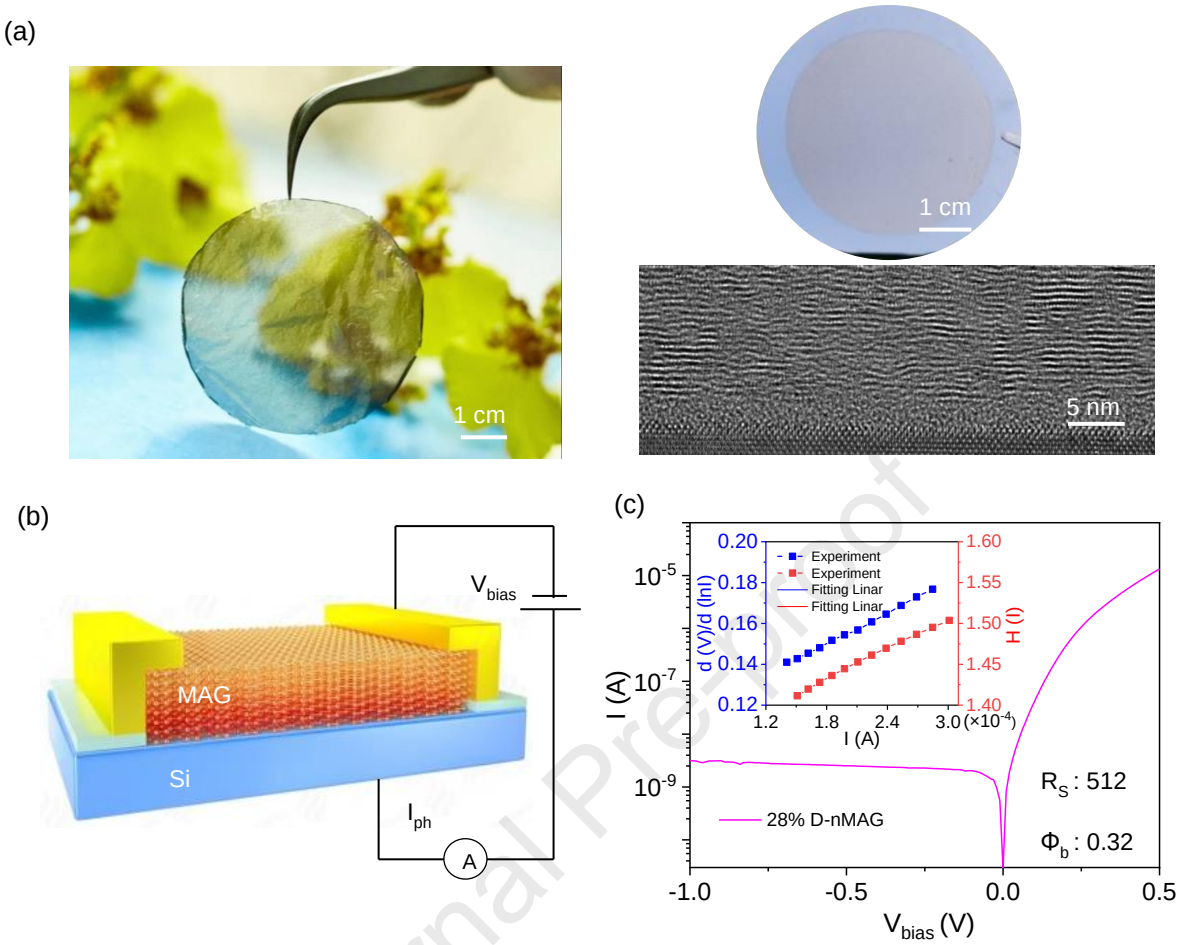

Fig. 2. Characterization of D-nMAG/Si photodetector. (a) The photo of the D-nMAG/Si wafer (2-inches) and HR-TEM image of D-nMAG/Si. (b) Device schematic. (c) The dark current of D-nMAG/Si. Inset: Extraction of D-nMAG/Si device parameters.

Journal Pre-proof

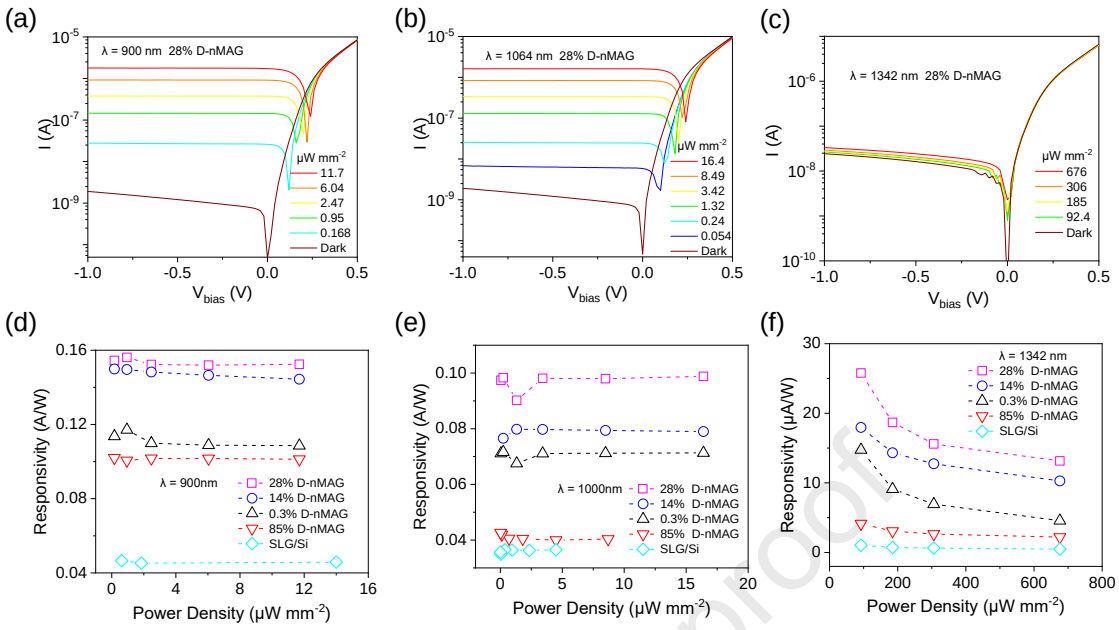

Fig. 3. Characterization of D-nMAG/Si photodetector under continuous laser illumination at NIR. (a, b, c) The I-V curve of 28% D-nMAG/Si with different laser power densities under dark and continuous laser illumination at 900 nm, 1064 nm, and 1342 nm wavelength. (d, e, f) The responsivity of D-nMAG/Si as a function of laser power density at NIR.

Journal Pre-proof

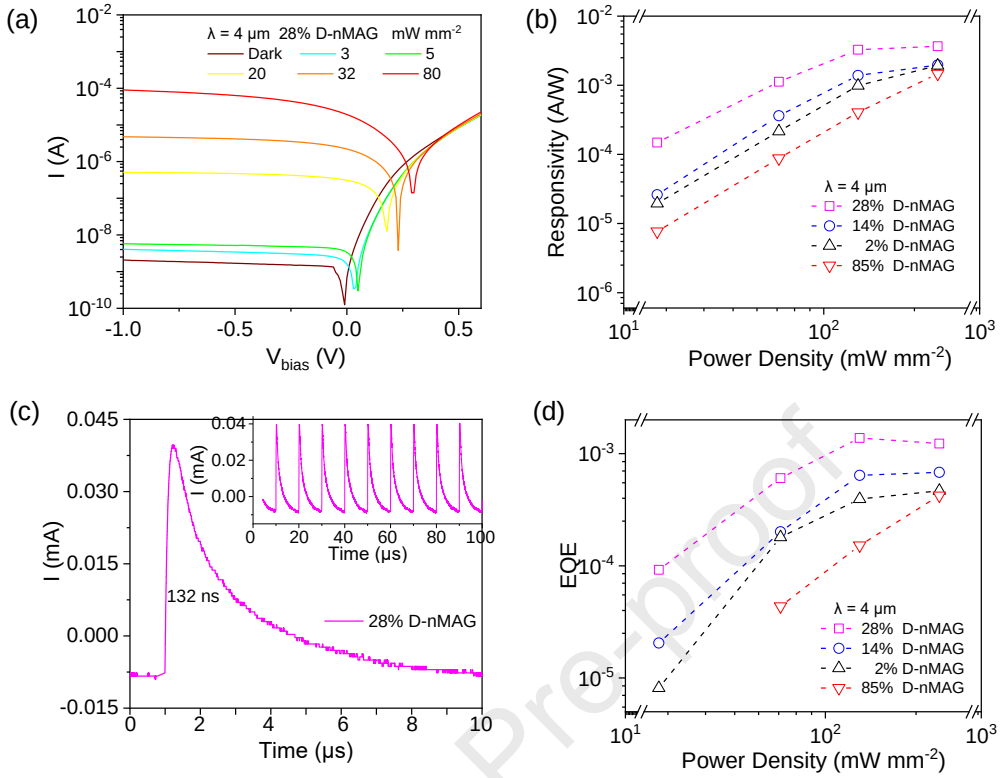

Fig. 4. Characterization of D-nMAG/Si photodetector under laser illumination at MIR. (a) The I-V curve of 28% D-nMAG/Si with different laser power densities under dark and laser illumination at 4 μm wavelength (200 fs pulse width, 100 kHz repetition rate). (b) The transient photo-response and periodic photocurrent peaks of 28% D-nMAG/Si under laser illumination at 4 μm wavelength with a fixed peak power density of 2×10^9 mW/mm^2 (average power density, 28 mW/mm^2). (c, d) The responsivity and EQE of D-nMAG/Si as a function of laser power density under laser illumination at 4 μm wavelength.

Journal Pre-proof

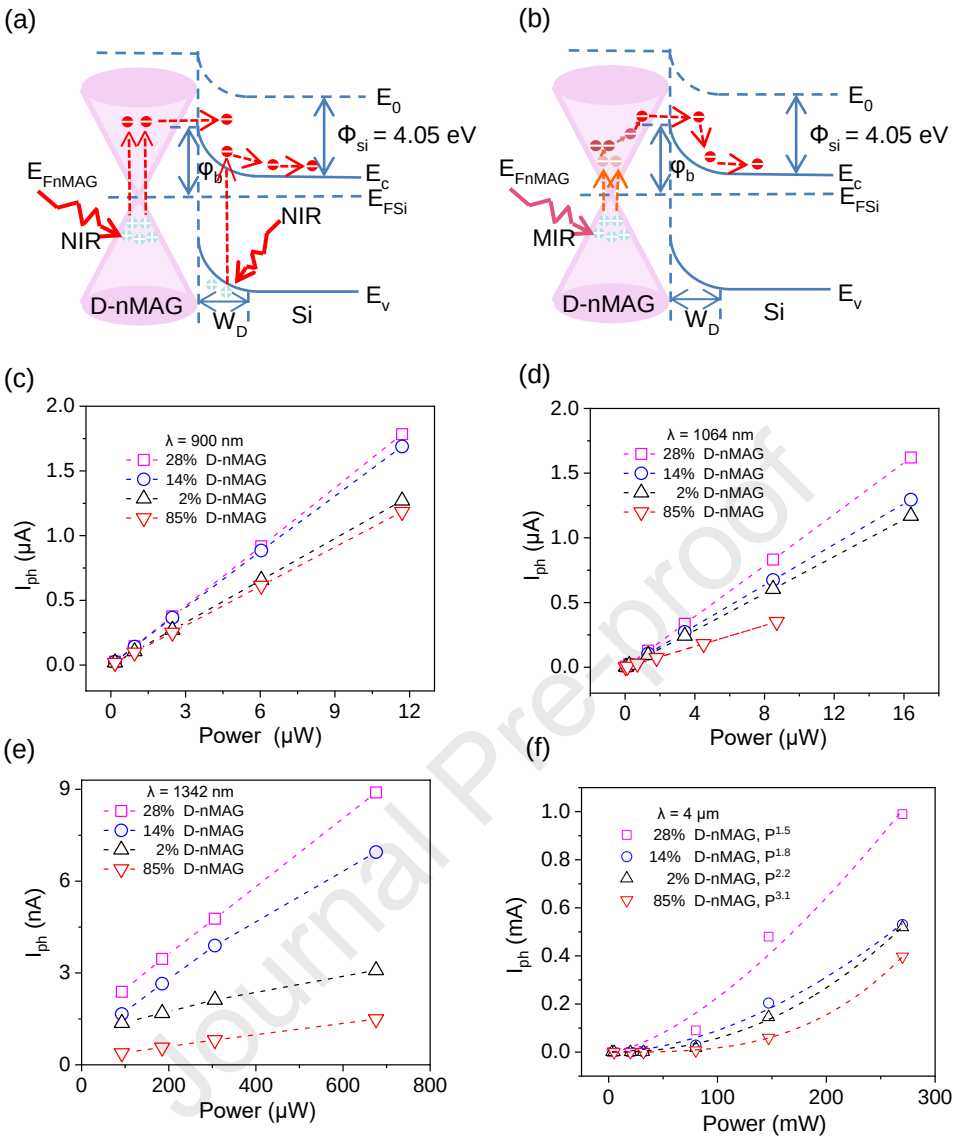

Fig. 5. (a, b) The energy band diagram structure of D-nMAG/Si photodetector at NIR and MIR regions. (c, d, e) The photocurrent current of D-nMAG/Si as a function of illumination power at 900 nm, 1064 nm, and 1342 nm wavelength, respectively. (f) The photocurrent current of D-nMAG/Si as a function of illumination power at 4 μm wavelength.

Journal Pre-proof

3.2 Photodetection behavior of D-nMAG/Si in NIR and MIR wavelength

We fabricated D-nMAG/Si devices (**Fig. 2b**) using 500-μm-thick, lightly-n-doped (10^{15} cm^{-3}) silicon substrates with 300 nm SiO_2 and the silicon window is 1 × 1 mm^2. With the assistance of water, D-nMAG can be directly transferred and affixed to a silicon wafer by tweezers (**Fig. 2a** and **Fig. S2 c-d**). This transfer approach avoids complicated operations and chemical residues during the transfer and etching processes (PMMA and metal ions, respectively). The clean heterojunction with van der Waals contacts of D-nMAG and silicon at an atomic level has been proved by HR-TEM cross-sectional image (**Fig. 2a** and **Fig. S2 a-b**).

The HR-TEM images also confirm the existence of defects in the D-nMAG. The relatively low Schottky barrier height (SBH) of D-nMAG/Si (~0.32 eV, **Fig. 2d**) verifies the capability for the detection of IR light with an energy lower than the bandgap of Si (~1.2 eV). The laser intensity-dependent temporal photoresponse tests of D-nMAG/Si devices have been assessed at NIR and MIR laser-wavelength, as shown in **Fig. 3** and **Fig. 4**, respectively. The photoresponse of the 28% D-nMAG/Si detector with the radiation power under 900 nm, 1064 nm, and 1342 nm wavelength exposure is graphically depicted in **Fig. 3a**, **b**, and **c**, respectively. At these wavelengths, the device saturation current increases with increasing power density, while the responsivity decrease with increasing wavelength due to the photon energy of the radiation light. The responsivity of D-nMAG/Si can reach 0.156 A/W @900 nm and 98 mA/W @1064 nm, which is 3 times higher than that of SLG/Si (**Fig. 3d** and **e**). The wavelength of 1342 nm exceeds the absorption cut-off of silicon, in this case, graphene as the main functional layer. Infrared radiation excites graphene to produce photogenerated carriers, and the carriers above the potential barrier can directly leap migration into silicon, forming photocurrents in the circuit. The responsivity of D-nMAG/Si can reach 25.7 μA/W at the wavelength of 1342 nm, which is more than an order of magnitude higher

than SLG/Si (**Fig. 3f**). Besides, the detailed characteristics of 14%, 2%, 47%, and 85% D-nMAG/Si devices in NIR wavelength can be found in **Fig. S5-8**. From these results, it is straightforward to find that the relationship between the defect-state content of D-nMAG and the corresponding responsivity of D-nMAG/Si devices in NIR is: 28% D-nMAG/Si > 14% D-nMAG/Si > 2% D-nMAG/Si > 47% D-nMAG/Si > 85% D-nMAG/Si (**Fig. 3d-f, S8**). Therefore, a certain amount of defect state facilitates the enhancement of the infrared detection of the device.

In addition to NIR radiation, the MIR infrared photoresponse of D-nMAG/Si was also studied using a laser of 4 μm wavelength (200 fs pulse width, 100 kHz repetition rate). The temporal photoresponses of 28% D-nMAG/Si with different light intensities are shown in **Fig. 4a**. The photocurrent rises as the pulsed infrared laser irradiates the device, quickly reaching peak photocurrent (**Fig. 4b**). The response time of this photodetector is 132 ns, defined as the time required to reach 90% of its peak photocurrent value from its 10%. The responsivity can reach 3.7 mA/W (**Fig. 4c**), and the corresponding external quantum efficiency (EQE) is 0.12% (**Fig. 4d**). Furthermore, the specific characteristics of the 14%, 2% and 85% D-nMAG/Si devices have been finely characterized in **Fig. S9-10**, which also reveals the same consequence as for the NIR wavelengths, *i.e.*, the responsivity of D-nMAG follows the sequence of 28% D-nMAG/Si > 14% D-nMAG/Si > 2% D-nMAG/Si > 85% D-nMAG/Si.

3.3 Detection Mechanism

D-nMAG is superior to infrared detection from the above detection results than SLG. D-nMAG (45 nm) has a stronger light absorption in a wide spectral range than SLG due to more layers. Silicon and D-nMAG are used simultaneously as the main functional layer at $\lambda < 1.1$ μm, where the light is excited through D-nMAG and silicon to produce carriers. For the photon energy of $0.5\ h\nu >$ SBH (*i.e.*, 2.1 μm > λ > 1.1 μm), the photon energy is not sufficient to excite carriers

in Si. The carriers excited in D-nMAG dominate the photoresponse. Photo-excited electrons directly transfer over the barrier between D-nMAG and Si and contribute to the photocurrent through the internal photoemission (IPE) effect[47], as shown in **Fig. 5a**. Under laser illumination at 4 μm wavelength (0.5 hν < SBH), the energy of photo-excited electrons is lower than SBH, preventing the direct injection of photogenerated carriers into silicon. On this occasion, the photo-excited electrons in D-nMAG thermalize into a Fermi-Dirac distribution (**Fig. 5b**). The thermalized high-energy hot electrons (hν > SBH) can emit into silicon via PTI (photo-thermionic) emission[41]. This is an essential characteristic of the D-nMAG/Si photodetector since the detection limit of photon energy is no longer governed by the bandgap of semiconductors but by the barrier height of the heterostructure. These two mechanisms can be confirmed by the relationship between photocurrent (I_{ph}) and laser power, as shown in **Fig. 5c-d**. The photocurrent was fitted with a power-law of $I_{ph} \propto \alpha P^{\beta}$, which shows a linear to super-linear transition as the photon energy decreases. It demonstrates a shift in the dominance of the photoelectric effect from the IPE effect to the PTI effect. [48]

Moreover, new scattering centers can be introduced due to the defective states in D-nMAG. It can effectively solve the challenges of low charge separation efficiency and severe carrier compounding caused by the zero-band gap of D-nMAG, thus further improving the detection capability of D-nMAG-based infrared devices[49-51]. In addition, the photogenerated carriers get trapped in defect states and enter CB or VB again to be thermalized. Then a new thermal equilibrium of carriers is established between the CB and the trap states, which process we defined as decompounding. This decompounding process can generate a photocurrent gain and further improve the performance of the detectors. As a result, high infrared absorption and trap-assisted gain increase EQE and responsivity of the D-nMAG-based infrared photodetector. Noteworthy,

excessive defect density can substantially reduce the state's density near the Fermi energy level of the material and decrease infrared detection performance. The performance of the devices is maximized only at a specific defect density, which can be confirmed in **Fig. 5c-f**. The ranking of β values obtained by fitting the normalized I_{ph} of D-nMAG/Si as a function of normalized illumination power is listed as follows: 28% D-nMAG/Si (β = 1.5) < 14% D-nMAG/Si (β = 1.8) < 2% D-nMAG/Si (β = 2.2) < 85% D-nMAG/Si (β = 3.1), which indicates that more high-energy electrons are available to leap into silicon in the 28% D- nMAG device. This result is consistent with the responsivity and EQE in **Fig. 3** and **4**.

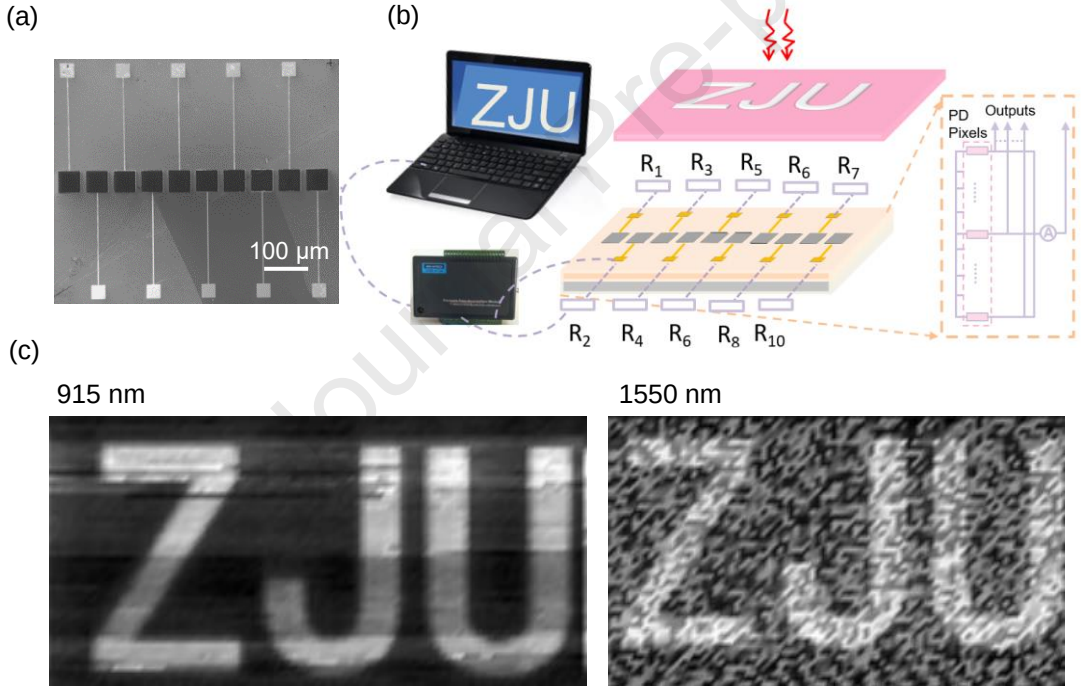

Fig. 6 . (a) The SEM image of the D-nMAG/Si line array device. (b) The imaging schematic of the line array device. (c) The photograph of "ZJU" imaged by line array devices at 915 nm and 1550 nm wavelength with 2 mW/mm^2 power density, respectively.

3.4 D-nMAG/Si image sensor

Large-area preparation of D-nMAG with low energy consumption lays the foundation for large-scale integration of array devices. Here, we show a 1 ×10 pixels line array image sensor, which exhibits excellent homogeneity, as depicted in **Fig. S13**. The TEM (**Fig. 6a**) confirmed that we had explored a nondestructive plasma etching technique for thick film materials. We collected the photocurrent and position information of the linear array through a data acquisition system while moving the object (ZJU masker) on a programmable X-Y stage (**Fig. 6b**). The photocurrents at the corresponding scan positions are then collected in a matrix to get high-resolution images at room temperature (**Fig. 6c**). Our work provides a promising carbon-based material to prepare large-scale, broad-spectrum imaging sensors.

4. Conclusion

A defect-state tunable carbon-based film with the features of low energy consumption, wafer-scale preparation, and compatibility with the CMOS production chain was fabricated. This work prepared photodetectors by heterogeneous integration of D-nMAG with silicon and constructed a defect engineering of D-nMAG to achieve ultra-fast (132 ns) broad-spectrum photodetection in the wavelength range from NIR to MIR. The photoresponsivity can reach to 0.156 A/W @ 900 nm and 3.7 mA/W @ 4 μm. Our work also explored a nondestructive plasma etching technique for patterning wafer-scale films to prepare carbon-based array photodetectors. Furthermore, this imaging sensor can obtain high-resolution images in IR wavelength at room temperature. Our demonstration provides material support for applying low-cost, broad-spectrum, high-performance infrared photodetectors.

Journal Pre-proof

Author information

Corresponding Author

*Yang Xu - School of Micro-nanoelectronics, State Key Laboratory of Silicon Materials, Hangzhou Global Scientific and Technological Innovation Center (HIC), ZJU-UIUC Joint Institute, Zhejiang University, Hangzhou, 310000, China; yangxu-isee@zju.edu.cn.

*Wenzhang Fang - MOE Key Laboratory of Macromolecular Synthesis and Functionalization, Department of Polymer Science and Engineering, International Research Center for X Polymers, Zhejiang University, Hangzhou, 310000, China; wenzhang.fang@zju.edu.cn.

*Chao Gao - MOE Key Laboratory of Macromolecular Synthesis and Functionalization, Department of Polymer Science and Engineering, International Research Center for X Polymers, Zhejiang University, Hangzhou, 310000, China; chaogao@zju.edu.cn.

Author Contributions

Xiaoxue Cao designed and conducted the experiments, interpreted the data, and drafted the manuscript. Wenzhang Fang proposed the study concept and revised the manuscript. Li Peng, Lixiang Liu, and Jianhang Lv contributed to the degradation experiment, analyzed the data, and revised the manuscript. Zongwen Li, Feng Tian, Yunfan Dong, Xinyu Liu, Ying Shen, and Haiyan Sun revised the manuscript. Chao Gao and Yang Xu supervised the study, reviewed the data, and revised the manuscript.

Declaration of competing interest

The authors declare no conflict of interest.

Acknowledgment

This work is supported by the National Natural Science Foundation of China (No. 52090030, 61874094, 92164106), Fundamental Research Funds for the Central Universities (No.

Journal Pre-proof

2021FZZX001-17 and K20200060), China Postdoctoral Science Foundation (2020M681819), ZJU Micro-Nano Fabrication Center. W. Fang thanks the financial support from the International Research Center for X Polymers, Zhejiang University.

Supporting Information.

Supplementary figures: HR-TEM image of D-nMAG/Si cross-section; the I-V curve of 14%, 2%, 85% D-nMAG/Si and SLG/Si with different laser power density under dark and continuous laser illumination at 900 nm, 1064 nm, and 1342 nm wavelength; the I-V curve of 14%, 2%, 85% D-nMAG/Si with different laser power density under dark and laser illumination at 4 μm wavelength (200 fs pulse width, 100 kHz repetition rate); the periodic photocurrent peaks and transient photo-response of 14%, 2%, 85% D-nMAG/Si under laser illumination at 4 μm wavelength with 32 mW/mm^2 power density; Demonstrate uniformity of line array devices under laser illumination at 1064 nm wavelength with 0.24 $\mu W\ mm^{-2}$ power density.

References

[1] G. Eda, G. Fanchini, M. Chhowalla, Large-area ultrathin films of reduced graphene oxide as a transparent and flexible electronic material, Nature nanotechnology 3(5) (2008) 270-274.

[2] S. Park, G. Wang, B. Cho, Y. Kim, S. Song, Y. Ji, M.-H. Yoon, T. Lee, Flexible molecular-scale electronic devices, Nature nanotechnology 7(7) (2012) 438-442.

[3] F.P. García de Arquer, A. Armin, P. Meredith, E.H. Sargent, Solution-processed semiconductors for next-generation photodetectors, Nature Reviews Materials 2(3) (2017) 1-17.

[4] W. Tian, T. Zhai, C. Zhang, S.L. Li, X. Wang, F. Liu, D. Liu, X. Cai, K. Tsukagoshi, D. Golberg, Low‐cost fully transparent ultraviolet photodetectors based on electrospun ZnO‐SnO2 heterojunction nanofibers, Advanced Materials 25(33) (2013) 4625-4630.

[5] K. Liu, M. Sakurai, M. Aono, D. Shen, Ultrahigh‐gain single SnO2 microrod photoconductor on flexible substrate with fast recovery speed, Advanced Functional Materials 25(21) (2015) 3157-3163.

[6] W. Tian, C. Zhang, T. Zhai, S.L. Li, X. Wang, J. Liu, X. Jie, D. Liu, M. Liao, Y. Koide, Flexible ultraviolet photodetectors with broad photoresponse based on branched ZnS‐ZnO heterostructure nanofilms, Advanced Materials 26(19) (2014) 3088-3093.

[7] J. Wang, C. Yan, M.-F. Lin, K. Tsukagoshi, P.S. Lee, Solution-assembled nanowires for high performance flexible and transparent solar-blind photodetectors, Journal of Materials Chemistry C 3(3) (2015) 596-600.

[8] X. Liu, L. Jiang, X. Zou, X. Xiao, S. Guo, C. Jiang, X. Liu, Z. Fan, W. Hu, X. Chen, Scalable Integration of Indium Zinc Oxide/Photosensitive‐Nanowire Composite Thin‐Film Transistors for Transparent Multicolor Photodetectors Array, Advanced Materials 26(18) (2014) 2919-2924.

[9] B.O. Jung, D.C. Kim, B.H. Kong, D.-W. Kim, H.K. Cho, Fully transparent vertically aligned ZnO nanostructure-based ultraviolet photodetectors with high responsivity, Sensors and Actuators B: Chemical 160(1) (2011) 740-746.

[10] Y.-L. Liu, C.-C. Yu, K.-T. Lin, T.-C. Yang, E.-Y. Wang, H.-L. Chen, L.-C. Chen, K.-H. Chen, Transparent, broadband, flexible, and bifacial-operable photodetectors containing a large-area graphene–gold oxide heterojunction, ACS nano 9(5) (2015) 5093-5103.

[11] P. LeVan, J. Long, C. Shott, J. Vincent, N. Tran, J. Mumolo, E. Luong, S. Rafol, J. Liu, A. Singh, 640x486 Long-Wavelength Two-Color GaAs/AlGaAs Quantum Well Infrared Photodetector (QWIP) Focal Plane Array Camera, (1999).

[12] J. Jimenez, X. Xiao, J. Sturm, P. Pellegrini, Tunable, long‐wavelength PtSi/SiGe/Si Schottky diode infrared detectors, Applied physics letters 67(4) (1995) 506-508.

Journal Pre-proof

[13] Y. Liu, J. Guo, E. Zhu, L. Liao, S.-J. Lee, M. Ding, I. Shakir, V. Gambin, Y. Huang, X. Duan, Approaching the Schottky–Mott limit in van der Waals metal–semiconductor junctions, Nature 557(7707) (2018) 696-700.

[14] T. Nishimura, K. Kita, A. Toriumi, Evidence for strong Fermi-level pinning due to metal-induced gap states at metal/germanium interface, Applied Physics Letters 91(12) (2007) 123123.

[15] C.W. Tan, K.H. Tan, Y.T. Ong, A.R. Mohamed, S.H.S. Zein, S.H. Tan, Energy and environmental applications of carbon nanotubes, Environmental Chemistry Letters 10(3) (2012) 265-273.

[16] D.K. Efetov, R.-J. Shiue, Y. Gao, B. Skinner, E.D. Walsh, H. Choi, J. Zheng, C. Tan, G. Grosso, C. Peng, Fast thermal relaxation in cavity-coupled graphene bolometers with a Johnson noise read-out, Nature nanotechnology 13(9) (2018) 797-801.

[17] S. Castilla, B. Terrés, M. Autore, L. Viti, J. Li, A.Y. Nikitin, I. Vangelidis, K. Watanabe, T. Taniguchi, E. Lidorikis, Fast and sensitive terahertz detection using an antenna-integrated graphene pn junction, Nano letters 19(5) (2019) 2765-2773.

[18] B. Fang, S.C. Bodepudi, F. Tian, X. Liu, D. Chang, S. Du, J. Lv, J. Zhong, H. Zhu, H. Hu, Bidirectional mid-infrared communications between two identical macroscopic graphene fibres, Nature communications 11(1) (2020) 1-9.

[19] M.-B. Lien, C.-H. Liu, I.Y. Chun, S. Ravishankar, H. Nien, M. Zhou, J.A. Fessler, Z. Zhong, T.B. Norris, Ranging and light field imaging with transparent photodetectors, Nature Photonics 14(3) (2020) 143-148.

[20] R.R. Nair, P. Blake, A.N. Grigorenko, K.S. Novoselov, T.J. Booth, T. Stauber, N.M. Peres, A.K. Geim, Fine structure constant defines visual transparency of graphene, Science 320(5881) (2008) 1308-1308.

[21] L. Liu, X. Cao, L. Peng, S.C. Bodepudi, S. Wu, W. Fang, J. Liu, Y. Xiao, X. Wang, Z. Di, R. Cheng, Y. Xu, C. Gao, B. Yu, Macroscopic-Assembled-Graphene Nanofilms/Germanium Broadband Photodetectors, 2021 IEEE International Electron Devices Meeting, (2021), 1-4.

[22] L. Peng, L. Liu, S. Du, S.C. Bodepudi, L. Li, W. Liu, R. Lai, X. Cao, W. Fang, Y. Liu, J. Lv, A. Muhammad, J. Liu, S. Jin, K. Wu, M. Lin, X. Cong, P. Tan, H. Zhu, Q. Xiong, X. Wang, W. Hu, X. Duan, B. Yu, Z. Xu, Y. Xu, C. Gao, Macroscopic assembled graphene nanofilms based room temperature ultrafast mid‐infrared photodetectors, InfoMat 4(6) (2022) e12309.

[23] L. Peng, Y. Han, M. Wang, X. Cao, J. Gao, Y. Liu, X. Chen, B. Wang, B. Wang, C. Zhu, Multifunctional Macroassembled Graphene Nanofilms with High Crystallinity, Advanced Materials 33(49) (2021) 2104195-2104203..

[24] F. Koppens, T. Mueller, P. Avouris, A. Ferrari, M. Vitiello, M. Polini, Photodetectors based on graphene, other two-dimensional materials and hybrid systems, Nature nanotechnology 9(10) (2014) 780-793.

[25] H. Fang, W. Hu, Photogating in low dimensional photodetectors, Advanced science 4(12) (2017) 1700323.

[26] Z. Chen, X. Li, J. Wang, L. Tao, M. Long, S.-J. Liang, L.K. Ang, C. Shu, H.K. Tsang, J.-B. Xu, Synergistic effects of plasmonics and electron trapping in graphene short-wave infrared photodetectors with ultrahigh responsivity, ACS nano 11(1) (2017) 430-437.

[27] A.H. Safavi-Naeini, T.P.M. Alegre, M. Winger, O. Painter, Optomechanics in an ultrahigh-Q two-dimensional photonic crystal cavity, Applied Physics Letters 97(18) (2010) 181106.

[28] G. Chung, C. Tin, J. Williams, K. McDonald, M. Di Ventra, S. Pantelides, L.C. Feldman, R. Weller, Effect of nitric oxide annealing on the interface trap densities near the band edges in the 4H polytype of silicon carbide, Applied Physics Letters 76(13) (2000) 1713-1715.

Journal Pre-proof

[29] K.S. Novoselov, L. Colombo, P. Gellert, M. Schwab, K. Kim, A roadmap for graphene, nature 490(7419) (2012) 192-200.

[30] Z. Hu, Z. Wu, C. Han, J. He, Z. Ni, W. Chen, Two-dimensional transition metal dichalcogenides: interface and defect engineering, Chemical Society Reviews 47(9) (2018) 3100-3128.

[31] Q. Li, Y. Zhao, C. Ling, S. Yuan, Q. Chen, J. Wang, Towards a comprehensive understanding of the reaction mechanisms between defective MoS2 and thiol molecules, Angewandte Chemie International Edition 56(35) (2017) 10501-10505.

[32] H. Nan, Z. Wang, W. Wang, Z. Liang, Y. Lu, Q. Chen, D. He, P. Tan, F. Miao, X. Wang, Strong photoluminescence enhancement of MoS2 through defect engineering and oxygen bonding, ACS nano 8(6) (2014) 5738-5745.

[33] F. Ceballos, M.-G. Ju, S.D. Lane, X.C. Zeng, H. Zhao, Highly efficient and anomalous charge transfer in van der Waals trilayer semiconductors, Nano Letters 17(3) (2017) 1623-1628.

[34] L. Britnell, R.M. Ribeiro, A. Eckmann, R. Jalil, B.D. Belle, A. Mishchenko, Y.-J. Kim, R.V. Gorbachev, T. Georgiou, S.V. Morozov, Strong light-matter interactions in heterostructures of atomically thin films, Science 340(6138) (2013) 1311-1314.

[35] Z. Yu, Y. Pan, Y. Shen, Z. Wang, Z.-Y. Ong, T. Xu, R. Xin, L. Pan, B. Wang, L. Sun, Towards intrinsic charge transport in monolayer molybdenum disulfide by defect and interface engineering, Nature communications 5(1) (2014) 1-7.

[36] S. Lyu, J. Schley, B. Loy, D. Lind, C. Hobot, R. Sparer, D. Untereker, Kinetics and time−temperature equivalence of polymer degradation, Biomacromolecules 8(7) (2007) 2301-2310.

Journal Pre-proof

[37] R.J. Crossley, P.J. Schubel, D.S. De Focatiis, Time–temperature equivalence in the tack and dynamic stiffness of polymer prepreg and its application to automated composites manufacturing, Composites Part A: Applied science and manufacturing 52 (2013) 126-133.

[38] L. Wenbo, Y. Ting-Qing, A. Qunli, Time-temperature-stress equivalence and its application to nonlinear viscoelastic materials, Acta Mechanica Solida Sinica-English Edition- 14(3) (2001) 195-199.

[39] F. Carbone, G. Aubock, A. Cannizzo, F. Van Mourik, R. Nair, A. Geim, K. Novoselov, M. Chergui, Femtosecond carrier dynamics in bulk graphite and graphene paper, Chemical Physics Letters 504(1-3) (2011) 37-40.

[40] I. Gierz, J.C. Petersen, M. Mitrano, C. Cacho, I. Turcu, E. Springate, A. Stöhr, A. Köhler, U. Starke, A. Cavalleri, Snapshots of non-equilibrium Dirac carrier distributions in graphene, Nature materials 12(12) (2013) 1119-1124.

[41] M. Massicotte, P. Schmidt, F. Vialla, K. Watanabe, T. Taniguchi, K.-J. Tielrooij, F.H. Koppens, Photo-thermionic effect in vertical graphene heterostructures, Nature communications 7(1) (2016) 1-7.

[42] M.T. Mihnev, J.R. Tolsma, C.J. Divin, D. Sun, R. Asgari, M. Polini, C. Berger, W.A. De Heer, A.H. MacDonald, T.B. Norris, Electronic cooling via interlayer Coulomb coupling in multilayer epitaxial graphene, Nature communications 6(1) (2015) 1-11.

[43] D. Brida, A. Tomadin, C. Manzoni, Y.J. Kim, A. Lombardo, S. Milana, R.R. Nair, K.S. Novoselov, A.C. Ferrari, G. Cerullo, Ultrafast collinear scattering and carrier multiplication in graphene, Nature communications 4(1) (2013) 1-9.

[44] S. Shallcross, S. Sharma, E. Kandelaki, O. Pankratov, Electronic structure of turbostratic graphene, Physical Review B 81(16) (2010) 165105.

Journal Pre-proof

[45] J. Berashevich, T. Chakraborty, Interlayer repulsion and decoupling effects in stacked turbostratic graphene flakes, Physical Review B 84(3) (2011) 033403.

[46] W. Landgraf, S. Shallcross, K. Türschmann, D. Weckbecker, O. Pankratov, Electronic structure of twisted graphene flakes, Physical Review B 87(7) (2013) 075433.

[47] J. Kniepert, D. Neher, Effect of the RC time on photocurrent transients and determination of charge carrier mobilities, Journal of Applied Physics 122(19) (2017) 195501.

[48] R. Kumar, M.A. Khan, A. Anupama, S.B. Krupanidhi, B. Sahoo, Infrared photodetectors based on multiwalled carbon nanotubes: Insights into the effect of nitrogen doping, Applied Surface Science 538 (2021) 148187.

[49] J. Jiang, C. Ling, T. Xu, W. Wang, X. Niu, A. Zafar, Z. Yan, X. Wang, Y. You, L. Sun, Defect engineering for modulating the trap states in 2D photoconductors, Advanced Materials 30(40) (2018) 1804332.

[50] Y. Yu, Y. Sun, Z. Hu, X. An, D. Zhou, H. Zhou, W. Wang, K. Liu, J. Jiang, D. Yang, Fast Photoelectric Conversion in the Near‐Infrared Enabled by Plasmon‐Induced Hot‐Electron Transfer, Advanced Materials 31(43) (2019) 1903829.

[51] S.K. Pradhan, B. Xiao, S. Mishra, A. Killam, A.K. Pradhan, Resistive switching behavior of reduced graphene oxide memory cells for low power nonvolatile device application, Scientific reports 6(1) (2016) 1-9.

Journal Pre-proof

1. A defect-state-tunable carbon nanofilm (D-nMAG) with unique features of low-cost, up to 45% light absorption in a broadband region, wafer-scale preparation, and compatibility with CMOS technology was fabricated.
2. D-nMAG/Si devices fully utilize the defect to achieve 0.156 A/W @ 900 nm and 3.7 mA/W @ 4 μm broad-spectrum photodetection with ultra-fast response (132 ns).
3. D-nMAG-based line array imaging sensor has been fabricated by a nondestructive plasma etching technique. It exhibits high-resolution infrared imaging of the target at room temperature.

Journal Pre-proof

Journal Pre-proof

Declaration of interests

☒ The authors declare that they have no known competing financial interests or personal relationships that could have appeared to influence the work reported in this paper.

☐ The authors declare the following financial interests/personal relationships which may be considered as potential competing interests:

Journal Pre-proof